KFUPM
Journal of Undergraduate Research International

Diamond Open Access 82

Article Geosciences

Glauconitic Greensand as a Sedimentary Source of Natural Hydrogen Generation: Experimental Insights and Implications for Basin Screening

Shahad Darwish and Anas Salisu*

Cite https://doi.org/10.64589/juri/231557

Submitted: April 24, 2026 Revised: May 7, 2026 Accepted: May 13, 2026

ABSTRACT

Natural hydrogen has been increasingly discussed as a low-carbon energy resource; however, most exploration concepts have focused on ultramafic rocks. This study conducted a screening case study of glauconitic sand from the Arnager Formation (Bornholm, Denmark) to assess its potential to generate natural hydrogen. The starting material was reacted with deionized water in sealed batch reactors for 24 h while varying the temperature (50–80 °C) and solid–liquid ratio (0.3–2) as a proxy for water–rock interaction. Gas chromatography showed that the gas produced was H2-dominant, with minor amounts of H2S and CO that varied with experimental conditions. The post-reaction mineralogy and bulk chemistry indicated a quartz-dominated framework that remained largely intact, whereas the Fe-bearing component showed evidence of selective modification: glauconite abundance decreased relative to the starting material, bulk Fe was depleted, and K was broadly retained in the solids. Together, these observations support a transferable concept: quartz-rich sands can act as redox-active substrates for hydrogen generation if they contain a reactive Fe-bearing fraction and are in contact with water at a favorable temperature and water–rock ratio.

Keywords: natural hydrogen; glauconite; greensand; water–rock reaction; energy transition

1. INTRODUCTION

Hydrogen is widely viewed as a decarbonization energy carrier, because it can supply low-carbon energy to sectors such as high-temperature industrial heat, refining, chemicals, and seasonal or long-term energy storage [1–3]. Currently, most hydrogen is produced industrially. In contrast, natural hydrogen is generated and accumulated in the subsurface, potentially allowing direct extraction [4,5]. Increasing reports of naturally occurring hydrogen have accelerated interest in identifying additional settings that can generate and retain H_2 at meaningful scales.

The dominant conceptual template for natural hydrogen generation is serpentinization, in which hydration of ultramafic rocks drives oxidation of ferrous [Fe(II)] to ferric [Fe(III)] iron and produces H2 [1,4–8]. Although serpentinization is commonly associated with ultramafic lithologies, in general, hydrogen generation depends on (i) the presence of redox-active Fe(II), (ii) water accessibility to Fe-bearing substrate, and (iii) thermodynamic and kinetic conditions that allow Fe-water electron transfer from [8,9]. Thus, hydrogen generation may occur across a wider range of lithologies than in ultramafics, provided available reactive Fe and circulating fluids through the host rock or sediment.

Sedimentary basins are attractive targets because they are widely distributed, frequently well-characterized by subsurface datasets, and commonly associated with existing infrastructure [10–12]. However, the hydrogen-generation potential of Fe-bearing sedimentary minerals remains poorly understood. Glauconite, a hydrous K- and Fe-rich phyllosilicate formed in marine settings, is a relevant candidate because it can host mixed-valence Fe within a clay lattice and is abundant in greensands [13–15]. Glauconite is typically hosted in quartz-rich sandstones where the framework grains are comparatively inert; therefore, any redox-driven H_2 generation should localize in the glauconite-bearing fraction [16,17]. This mineralogical simplicity provides an opportunity to link gas composition to the selective alteration of Fe-bearing components.

This study emphasized screening logic rather than a full-play assessment. Specifically, we tested whether glauconitic greensand could produce an H_2-rich headspace gas mixture during short-duration water–rock interaction at low-to-moderate temperatures and evaluated how H_2 purity responds to temperature and water–rock contact. The gas composition trends were interpreted against post-reaction mineralogical and geochemical tracers.

2. MATERIALS AND GEOLOGICAL CONTEXT

The study used glauconitic greensand from the Arnager Greensand Formation on the southern coast of Bornholm Island, Denmark (Figure 1) [18]. The Arnager unit is quartz-rich sand with abundant glauconite pellets that impart a characteristic green

Published under an exclusive license by KFUPM

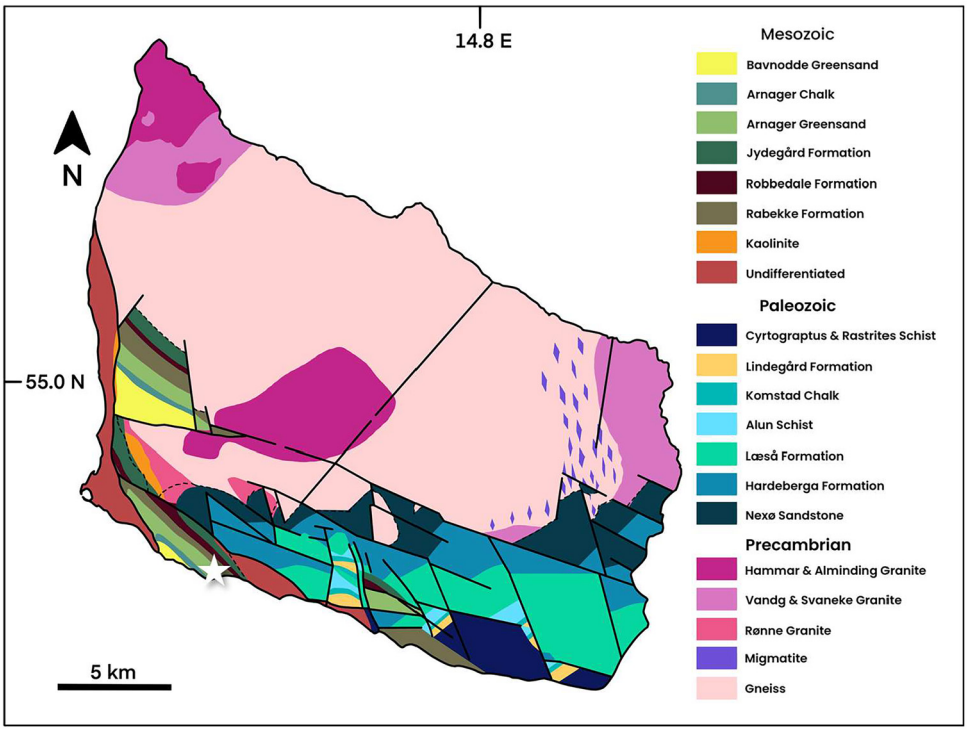


Figure 1. Geologic map of Bornholm Island, Denmark. The white star indicates the location at which samples were collected from the Arnager Greensand

color. This combination of an inert quartz framework with an Fe-bearing authigenic clay fraction makes the sediment a practical natural substrate for investigating hydrogen generation during controlled water–rock interactions. Glauconite is a K- and Fe-rich phyllosilicate that is structurally related to illite/mica and can contain Fe in multiple valence states. In principle, residual Fe(II) sites can participate in oxidation reactions during interactions with water, providing electrons that reduce water to H_2 [19–21]. As glauconite is common in marine shelf successions and condensed sections, it represents a transferable mineral target that can be evaluated in multiple basins using existing stratigraphic and reservoir datasets.

3. METHODOLOGY

The experimental program was designed as a screening matrix to isolate the first-order controls on gas composition during water–rock interactions, that is, temperature (which governs the reaction kinetics) and water–rock contact (represented by the solid–liquid ratio, S/L) (Table 1). All experiments used the same starting material and run duration to facilitate comparison of gas compositions across conditions. Full conditions are described in the following sections.

3.1. Batch Reactor Experiments. The experiments were conducted in multiposition magnetically stirred stainless steel reactors (500 mL internal volume) (Figure 2). For each run, 10 g of greensand was loaded into the reactor, followed by deionized water volumes selected to achieve solid–liquid ratios of 0.3, 0.5, 1.0, and 2.0 (Table 1). The reactors were sealed and evacuated prior to heating to minimize atmospheric contamination and to ensure that the measured headspace gases were generated by the water–rock reaction. Each experiment was held for 24 h at a target temperature of 50 or 80 °C (Table 1) before being cooled to room temperature. Following the reaction, the headspace gas was sampled and analyzed using gas chromatography. As the post-reaction pressures were low, nitrogen was used to pressurize the reactor to enable gas retrieval. Therefore, the analytical emphasis in this study was on the relative gas composition in the mixture (percentage fractions) rather than the absolute gas yield, which would require robust pressure-volume quantification. This composition-first approach is appropriate for a screening study aimed at identifying H_2-forward operating windows and highlighting impurity behavior (e.g., H_2S and CO) relevant to gas quality.

3.2. Solid Characterization. To relate the gas composition to the mineral reactions, the reacted solids were separated

Table 1. *Experimental conditions*

Sample Code	Sand Amount (g)	Liquid Amount (ml)	Temperature (°C)
S1	10.0	5.0	50
S2	10.0	10.0	50
S3	10.0	20.0	50
S4	10.0	30.0	50
S5	10.0	5.0	80
S6	10.0	10.0	80
S7	10.0	20.0	80
S8	10.0	30.0	80

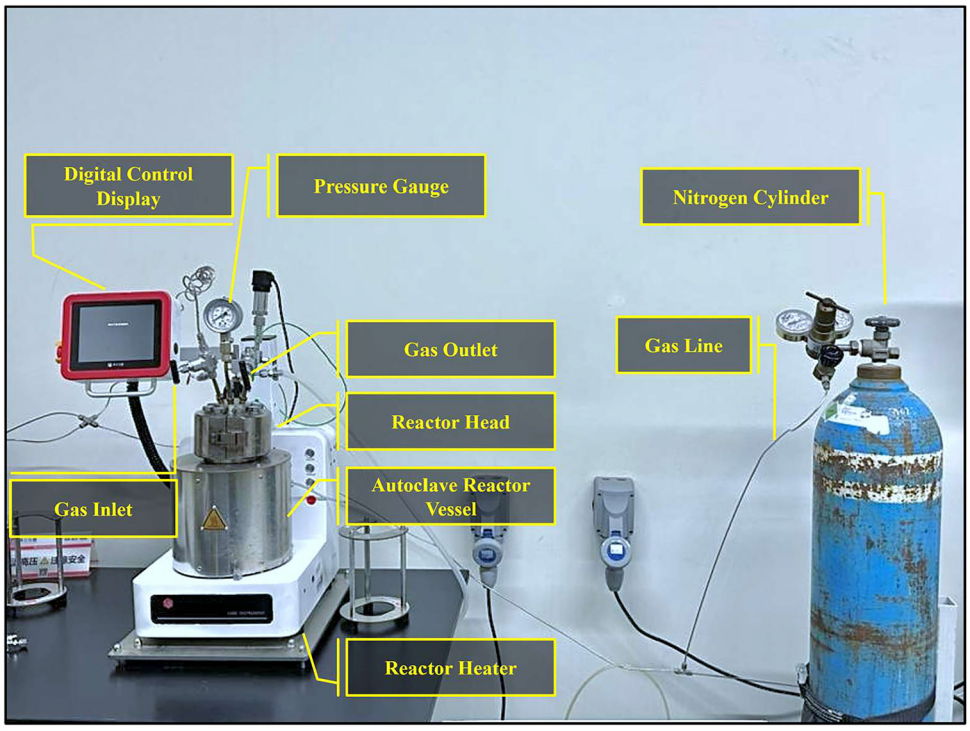


Figure 2. Experimental setup of hydrothermal reactors

from the aqueous phase after each run, then dried, and characterized using complementary mineralogical and geochemical methods**.** Scanning electron microscope (SEM) analysis coupled with energy-dispersive X-ray spectroscopy (EDS) was used to examine the grain morphology and elemental distribution in the sand pre- and post-reaction. Analyses were performed using a Zeiss Gemini 550 SEM equipped with an Aztec EDS system. Samples of unconsolidated sand were mounted on aluminum stubs with carbon adhesive tabs and sputter-coated with a ~30-nm gold layer using a Quorum Q150R coater to ensure electrical conductivity. SEM imaging and EDS measurements were performed at an accelerating voltage of 10–15 kV and probe current of ~1–2 nA**.**

Mineralogical changes in the starting and post-reaction solids were evaluated using powder X-ray diffraction (XRD) using a Malvern PANalytical Empyrean diffractometer. The dried samples were gently disaggregated and ground into a fine, homogeneous powder. Diffraction patterns were collected using Cu Kα radiation over a 2θ range of 4–40°, and mineral phases were identified through comparison with standard reference patterns from established databases. Bulk chemical changes were assessed by wavelength-dispersive X-ray fluorescence (XRF) using a PANalytical Zetium spectrometer (Malvern PANalytical, Almelo, Netherlands). Finely powdered samples were converted to fused glass beads using lithium metaborate flux ($LiBO_2$:$Li_2B_4O_7$, 49.75:49.75:0.50) in Pt-Au crucibles with a Classie OX Advanced fusion system following a standard heating program (hold at 500 °C, ramp to 1125 °C with rocking). Subsequently, the major and minor elements were quantified using certified reference materials (WROXI series), and data acquisition and matrix corrections were performed using PANalytical SuperQ (v6).

4. RESULTS AND DISCUSSION

4.1. Starting Material Characterization. Pre-reaction observations indicated that the greensand was dominated by quartz with glauconite present as pellet-like grains (Figure 3b, c). SEM and EDS analyses confirmed that glauconite was enriched in Fe and K relative to quartz. This result is consistent with glauconite being the primary candidate for redox-active behavior within the sample (Figure 3d). Bulk XRD analysis confirmed quartz as the dominant phase and identified glauconite as a significant minor component, along with feldspar and mica phases (Table 2, Figure 4).

4.2. Headspace Gas Composition (Screening Outcome). Across the experimental matrix, the reaction of glauconitic greensand with deionized water generated a measurable headspace gas mixture dominated by H_2 (Figure 5), confirming that a quartz-rich sediment can produce hydrogen-rich gas when it contains a reactive Fe-bearing fraction. Although H_2 constitutes the principal component in most runs, the headspace also contained minor amounts of H_2S and CO**,** and the relative abundance of these impurities varied systematically with both temperature and S/L (Figure 5), indicating that gas quality is controlled by coupled redox and speciation processes rather than by a single variable.

Two screening level patterns were observed. First, increasing temperature strengthened H_2 dominance and expanded the range of S/L conditions under which the product gas remains hydrogen-forward (Figure 5). At low temperatures, the outcomes are more sensitive to water–rock contact, and the system can shift toward mixed-gas compositions under certain S/L states. However, with moderate heating, H_2 remains the prevailing component across most of the tested S/L range. This is consistent

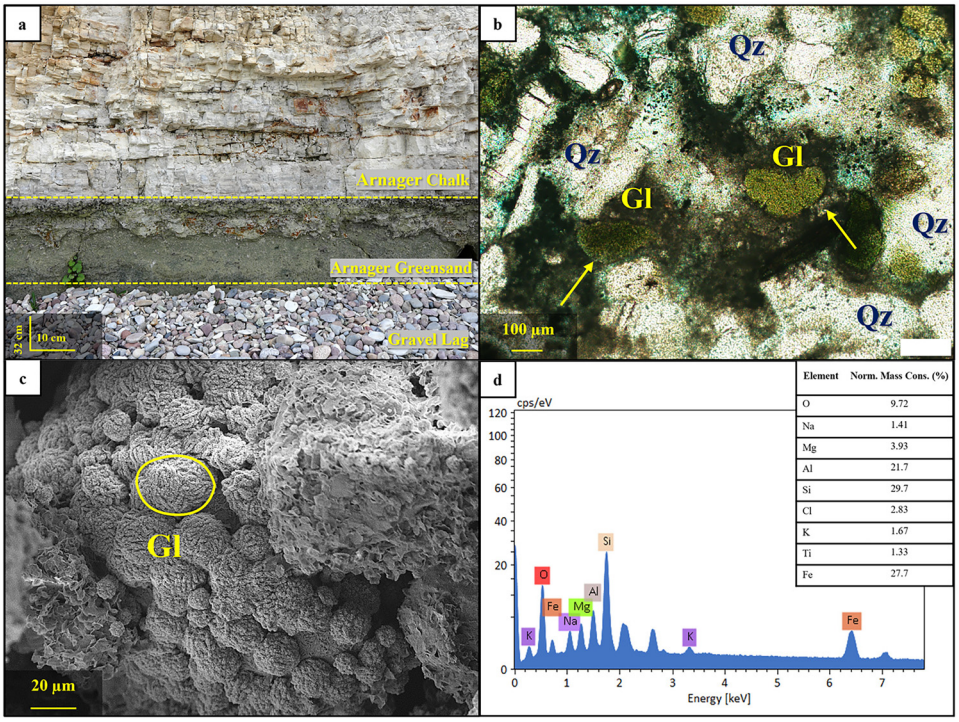


Figure 3. (a) Outcrop photograph of the sampled material showing the greensand unit overlain by chalk layer. (b) Thin-section image highlighting the green glauconite grains (Gl), surrounded by colorless, low relief grains that represent quartz (Qz). (c) SEM photomicrograph of glauconite pellets. (d) EDS spectrum highlighting the elemental composition by mass of glauconite in the analyzed sample (yellow circle in c)

Table 2. *Mineralogical composition from XRD analysis*

Sample ID	Quartz %	Calcite %	Microcline %	Muscovite %	Orthoclase %	Biotite %	Glauconite %	Pyrite %
S0	70.1	3.4	8.6	7.9	1.3	0.2	7.6	0.9
S1	71.8	2.2	9.2	10.0	2.0	0.5	4.3	
S2	71.6	2.6	7.9	9.2	1.8	0.5	6.4	
S3	73.1	2.3	7.9	9.6	1.6	0.6	4.9	
S4	74.8	2.1	7.3	9.2	1.9	0.6	4.1	
S5	75.1	1.4	7.1	7.3	1.9	0.5	6.7	
S6	74.1	2.9	6.1	9.7	1.8	0.7	4.7	
S7	73.5	1.8	7.8	9.1	2.2	0.4	5.2	
S8	75.0	2.2	6.6	8.6	2.6	0.7	4.3	

with temperature accelerating the kinetics of Fe-driven water reduction and associated mineral alteration reactions. This temperature effect suggests that hydrogen-forward behavior may be more robust in settings with modestly elevated temperatures (e.g., shallow-to-intermediate burial conditions) than in near-surface conditions.

Second, impurity expression is strongly condition-dependent, implying competition between hydrogen-generating pathways and secondary sulfur- and carbon-related reactions that can consume reducing capacity and/or partition products into the gas phase (Figure 5). The appearance of H_2S is consistent with sulfur cycling that involves trace sulfur-bearing components in the starting material and indicates that "souring" can become significant under particular water–rock contact conditions, potentially lowering H_2 purity despite the occurrence of hydrogen generation. Similarly, the variability in CO indicates that carbon speciation is sensitive to experimental conditions, likely reflecting shifts between dissolution/degassing and mineral trapping behaviors during the reaction. Collectively, these observations emphasize that the experiments are best interpreted as a gas-quality screening framework; temperature and S/L do not solely control gas production, but also govern whether the system yields a clean, H_2-rich mixture or more complex product gas where sulfur and carbon pathways are more strongly expressed.

4.3. Post-Reaction Mineralogy and Geochemistry.

Bulk XRD results showed that the reacted solids remained strongly quartz-dominated after 24 h, indicating that the mineralogy of the sand was largely preserved under the investigated conditions (Figure 4, Table 2). This persistence of quartz is expected, given its low reactivity at 50–80 °C, and supports the interpretation that the experiments did not drive the pervasive dissolution

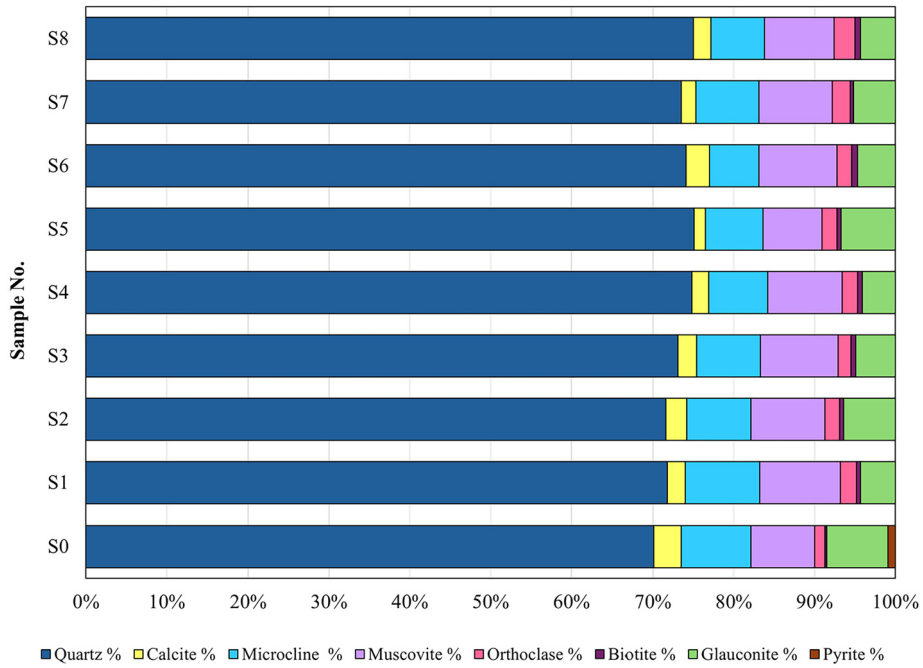


Figure 4. XRD patterns

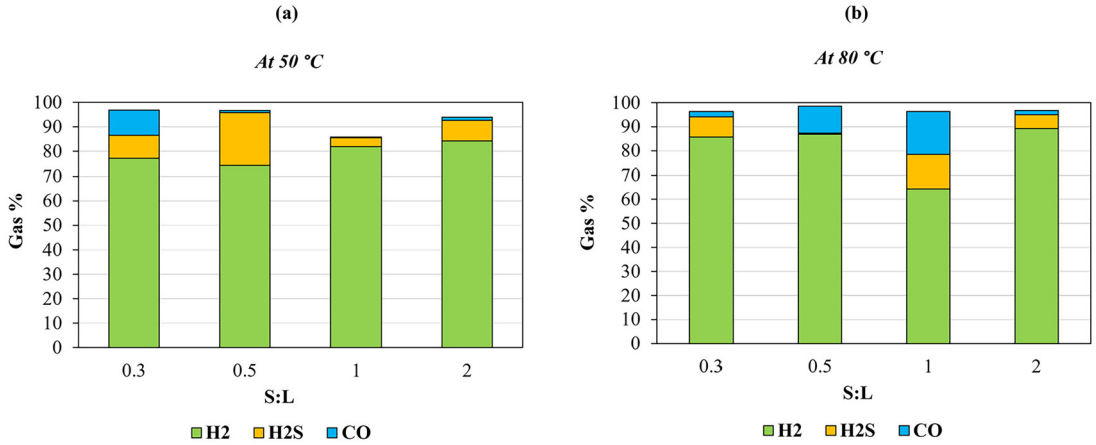


Figure 5. Headspace gas yields at each temperature with respect to different solid-liquid ratios; (a) 50 °C, (b) 80 °C

of the host sediment. Instead, the most consistent mineralogical change was a decrease in the glauconite abundance relative to the starting material, which was accompanied by a reduction in other reactive minor phases (Table 2). This shift is best explained by selective alteration and/or partial dissolution of the glauconite-bearing fraction, which hosts the majority of the reactive iron in the sample.

The XRF measurements provided independent and complementary geochemical constraints for this interpretation (Table 3, Figure 6). Across the experimental suite, the bulk Fe^{2+}/Fe^{3+} was depleted relative to the starting material, indicating that the reactive Fe^{2+}/Fe^{3+} budget was mobilized and/or redistributed during the reaction (Figure 6b). In contrast, K^{+} was broadly retained in the solid phase and exhibited comparatively modest variability (Figure 6a). Because K^{+} is a diagnostic component of glauconite, its retention suggests that the glauconite was not completely destroyed during the short experimental timeframe. The data are consistent with partial modification of glauconite, in which Fe-bearing sites are preferentially affected while the broader silicate framework (and its K^{+} content) remains partly preserved. In other words, the mineralogical (reduced glauconite abundance) and chemical (Fe^{2+}/Fe^{3+} depletion) signals lead to the same conclusion: the most reactive component is the Fe-bearing glauconitic fraction and not the quartz-rich framework.

Taken together, the XRD and XRF results support a reaction pathway in which the system behaves as an "inert framework + reactive minor fraction" assemblage. Quartz largely functions as a stable host phase, whereas the glauconite-bearing component undergoes preferential transformation, supplying redox-active Fe that is mechanistically linked to hydrogen generation. This selective alteration model was also consistent with the observed gas

Table 3. *Average mass percentage of K^+ % and Fe^{2+}/Fe^{3+} % obtained from XRF*

Sample Code	Sand : Liquid	Temperature (°C)	K^+ %	Fe^{2+}/Fe^{3+} %
S0	—	—	7.3	20.2
S1	1:0.5	50	7.0	14.2
S2	1:1	50	8.9	15.2
S3	1:2	50	7.6	19.0
S4	1:3	50	8.4	15.2
S5	1:0.5	80	9.4	17.9
S6	1:1	80	7.3	15.6
S7	1:2	80	8.2	15.3
S8	1:3	80	7.7	16.3

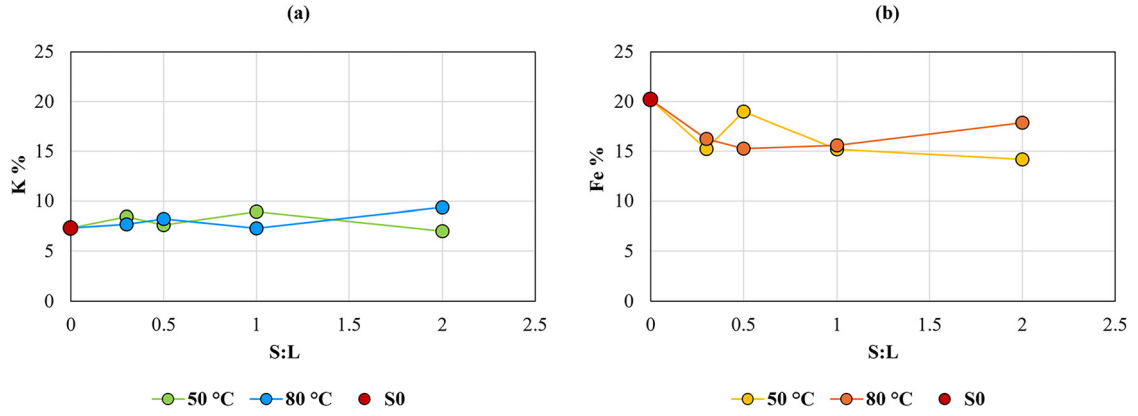


Figure 6. XRF patterns of K^+ % (a) and Fe^{2+}/Fe^{3+} % (b)

outcomes, in which hydrogen-rich mixtures were produced, with no evidence of extensive bulk sediment dissolution.

4.4. Relevance to Natural Hydrogen Exploration.

The screening results demonstrate that quartz-rich sediment can generate an H_2-dominant gas mixture when it contains a reactive Fe-bearing fraction (glauconite) and water–rock interactions occur under favorable thermal and contact conditions. This supports a sedimentary analog to serpentinization: hydrogen generation is controlled by the accessibility and redox transformation of Fe (II) rather than requiring ultramafic lithologies[8]. In this study, the quartz framework largely persisted, indicating that the reaction was not driven by the bulk dissolution of the host sediment. Instead, Fe depletion and reduced glauconite abundance indicate that the glauconite-bearing fraction was the most reactive component during the experimental timeframe.

Additionally, temperature exerts a clear screening effect by accelerating reaction kinetics and broadening the range of conditions under which H_2 remains the dominant gas. Used as a proxy for water–rock contact, the solid–liquid ratio modulates the expression of minor gases and influences H_2 purity. The presence of H_2S and CO, even as minor components, highlights that gas quality is an essential part of any natural hydrogen assessment[5,9]. Sulfur availability, fluid composition, and the ability of Fe-bearing phases to capture sulfide as solids likely influence whether the produced gas remains H_2-rich or sours[9]. Similarly, carbon-bearing gases reflect inorganic carbon speciation and mineral trapping behavior, which can change with temperature and the water–rock ratio.

From an energy transition standpoint, the principal value of this study is the development of a transferable screening concept for sedimentary basins. Glauconite-bearing intervals are widely mapped in stratigraphy and petroleum system studies[20–24], and many basins already have core, cutting, log, and mineralogical datasets that can be repurposed to identify candidate intervals where reactive Fe-bearing minerals coincide with favorable temperature windows and fluid access.

4.5. Limitations and Future Work.

It is essential to note that this study did not intend to quantify subsurface flux or reservoir-scale accumulation. Instead, the primary goal was to investigate the potential of hydrogen generation form iron-rich shallower lithologies, such as the glauconitic sand, rather than deeper, commonly targeted ultramafic rocks. However, this study provides a practical basis for prioritizing targets for future work, including improved gas-yield quantification, reactive-transport tests under controlled fluid chemistry and further solid quantification through direct Fe-valence measurements.

Since the study is exploratory in nature, pressure of the gas was not quantified, as the pressure generated during the experiments was very low and approached the uncertainty limit of the pressure gauge. Therefore, the pressure measurements were not sufficiently reliable for accurate quantification. The experiments were conducted for only 24 h, and the temperature range was

limited to 50–80 °C, reflecting shallow subsurface conditions. Future work will focus on assessing the effects of temperature and experimental duration on reaction rates and their relationship to hydrogen production capacity. This will be achieved by extending the temperature range and increasing the experimental duration to maximize gas generation from the reaction. Consequently, hydrogen production potential will be evaluated by quantifying the total volume of gas produced rather than relying on headspace relative abundance. In addition, detailed measurements of Fe^{2+}/Fe^{3+} ratio are a future objective that may provide further insights into material reactivity.

5. CONCLUSIONS

This study conducted a screening case study of glauconitic sand from the Arnager Formation (Bornholm, Denmark) to assess its potential to generate natural hydrogen by examining water–rock interactions. Our findings include the following:

- Glauconite-bearing greensand generated H_2-dominant headspace gas during 24 h water–rock interaction experiments under mild hydrothermal conditions.
- The temperature strengthened hydrogen-forward gas composition across a wider range of water–rock contact states, supporting its role as a first-order screening control.
- Post-reaction solids remained quartz-dominant, indicating a limited alteration of the bulk sand framework over the experimental timeframe.
- Decreased glauconite abundance and systematic Fe depletion, coupled with broad K retention, indicated selective modification of the glauconite-hosted Fe-bearing fraction consistent with an Fe-driven redox contribution to H_2 generation.

In summary, glauconitic intervals in sedimentary basins should be considered as underexplored candidates for natural hydrogen screening, alongside the evaluation of impurity controls (H_2S, CO/CO_2), fluid chemistry, and reservoir/seal context.

AFFILIATIONS AND AUTHOR DETAILS

Undergraduate Author

Shahad Darwish – *College of Petroleum Engineering and Geosciences, King Fahd University of Petroleum & Minerals, Dhahran 31261, Saudi Arabia*; 0009-0008-2530-3231
Email: S202468980@kfupm.edu.sa

Corresponding Author

Anas Salisu – *Research Mentor, Research Scientist, Center for Integrative Petroleum Research, King Fahd University of Petroleum & Minerals, Dhahran 31261, Saudi Arabia*; 0009-0002-6134-0511
Email: Anas.salisu@kfupm.edu.sa

ACKNOWLEDGEMENTS

We acknowledge the College of Petroleum Engineering and Geosciences (CPG) at King Fahd University of Petroleum & Minerals for providing access to facilities and institutional support. We also thank Arabian Drilling for sponsoring the geological field trips during which the study samples were collected. We are grateful to Prof. Khalid Al-Ramadan, Dr. Isah Mohammed, and Dr. Ayman Al-Leyhani for their sustained guidance, constructive feedback, and support during this study. We additionally thank: Fatimah Al-Ibrahim, Fatimah Al-Shammary, Ayah Al-Khalifah, and Ayah Al-Aradi for their help with field sampling collection.

REFERENCES

(1) Wang, L., Jin, Z., Chen, X., Su, Y. & Huang, X. The Origin and Occurrence of Natural Hydrogen. *Energies 2023, Vol. 16, Page 2400* **16**, 2400 (2023).

(2) Torghabeh, A. K., Hashemi, S. H., Moghaddam, M. E., Kamali, M. & Pradhan, B. Natural hydrogen (white hydrogen) exploration methods and identification of sources: A comprehensive overview. *Gondwana Research* **155**, 107–119 (2026).

(3) Hassanpouryouzband, A. *et al.* Geological Hydrogen Storage: Geochemical Reactivity of Hydrogen with Sandstone Reservoirs. *ACS Energy Lett.* **7**, 2203–2210 (2022).

(4) Jackson, O. *et al.* Natural hydrogen: sources, systems and exploration plays. *Geoenergy* **2**, (2024).

(5) Zgonnik, V. The occurrence and geoscience of natural hydrogen: A comprehensive review. *Earth. Sci. Rev.* **203**, 103140 (2020).

(6) Dornelas, V. F. *et al.* Occurrences and Perspectives of Natural Hydrogen Extraction: The Brazilian Context. *Energies 2025, Vol. 18, Page 2859* **18**, 2859 (2025).

(7) Lefeuvre, N. *et al.* Characterizing Natural Hydrogen Occurrences in the Paris Basin From Historical Drilling Records. *Geochemistry, Geophysics, Geosystems* **25**, e2024GC011501 (2024).

(8) L.E., M., E.T., E., T.M., M., T.P., T. & A.S., T. Hydrogen generation from serpentinization of iron-rich olivine on Mars, icy moons, and other planetary bodies. *Icarus* **372**, 175–200.

(9) ning Tian, Q., qing Yao, S., juan Shao, M., Zhang, W. & hua Wang, H. Origin, discovery, exploration and development status and prospect of global natural hydrogen under the background of "carbon neutrality". *China Geology* **5**, 722–733 (2022).

(10) Worden, R. H. & Burley, S. D. Sandstone Diagenesis: The Evolution of Sand to Stone. in *Sandstone Diagenesis* 1–44 (2003). doi:https://doi.org/10.1002/9781444304459.ch.

(11) Capua, A. Di *et al.* From volcanoes to sedimentary systems. *Geol. Soc. Spec. Publ.* **520**, 1–9 (2023).

(12) Dowey, P. J., Worden, R. H., Utley, J. & Hodgson, D. M. Sedimentary controls on modern sand grain coat formation. *Sediment. Geol.* **353**, 46–63 (2017).

(13) Fernández-Landero, S. & Fernández-Caliani, J. C. Mineralogical and Crystal-Chemical Constraints on the Glauconite-Forming Process in Neogene Sediments of the Lower Guadalquivir Basin (SW Spain). *Minerals 2021, Vol. 11, Page 578* **11**, 578 (2021).

(14) Huggett, J. M. Minerals: Glauconites and Green Clays. *Reference Module in Earth Systems and Environmental Sciences* https://doi.org/10.1016/b978-0-12-409548-9.02893-1(2013)doi:10.1016/b978-0-12-409548-9.02893-1.

(15) Thompson, G. R. & Hower, J. The Mineralogy of Glauconite. *Clays and Clay Minerals 1975 23:4* **23**, 289–300 (1975).

(16) Zhang, Q. & Tutolo, B. M. Geochemical evaluation of glauconite carbonation during sedimentary diagenesis. *Geochim. Cosmochim. Acta* **306**, 226–244 (2021).

(17) Dasi, E., Rudmin, M. & Banerjee, S. Glauconite applications in agriculture: A review of recent advances. *Appl. Clay Sci.* **253**, (2024).

(18) Hart, M. B., Bromley, R. G. & Packer, S. R. Anatomy of the stratigraphical boundary between the Arnager Greensand and Arnager Limestone (Upper Cretaceous) on Bornholm, Denmark. *Proceedings of the Geologists' Association* **123**, 471–478 (2012).

(19) Baldermann, A. *et al.* The role of Fe on the formation and diagenesis of interstratified glauconite-smectite and illite-smectite: A case study of Lower Cretaceous shallow-water carbonates. *Chem. Geol.* **453**, 21–34 (2017).

(20) Diaz, E., Prasad, M., Mavko, G. & Dvorkin, J. Effect of glauconite on the elastic properties, porosity, and permeability of reservoir rocks. *The Leading Edge* **22**, 42–45 (2003).

(21) Tribovillard, N. *et al.* The contrasting origins of glauconite in the shallow marine environment highlight this mineral as a marker of paleoenvironmental conditions. *Comptes Rendus - Geoscience* **355**, (2023).

(22) Skiba, M., Maj-Szeliga, K., Szymański, W. & Błachowski, A. Weathering of glauconite in soils of temperate climate as exemplified by a Luvisol profile from Góra Puławska, Poland. *Geoderma* **235–236**, 212–226 (2014).

(23) Zhang, Q., Awolayo, A. N., Nightingale, M. J. & Tutolo, B. M. Kinetics of glauconite dissolution in anoxic conditions as a function of pH and temperature. *Geochim. Cosmochim. Acta* **336**, 78–91 (2022).

(24) BELL, D. L. & Goodell, H. G. A comparative study of glauconite and the associated clay fraction in modern marine sediments. *Sedimentology* **9**, 169–202 (1967).